JOURNAL OF AIRCRAFT
Vol. 33, No. 3, May–June 1996

Full-Scale Wind-Tunnel Studies of F/A-18 Tail Buffet

Larry A. Meyn*
NASA Ames Research Center, Moffett Field, California 94035
and
Kevin D. James†
Sterling Federal Systems, Inc., Palo Alto, California 94303

Tail buffet studies were conducted on a full-scale, production F/A-18 fighter aircraft in the 80 by 120 ft Wind Tunnel at NASA Ames Research Center. The F/A-18 was tested over an angle-of-attack range of 18–50 deg, and at wind speeds of up to 168 ft/s, corresponding to a Reynolds number of 12.3 × 10^6 based on mean aerodynamic chord and a Mach number of 0.15. The port, vertical tail fin was instrumented and the aircraft was equipped with a removable leading-edge extension (LEX) fence. Time-averaged, power-spectral analysis results are presented for the tail fin bending moment derived from the integrated pressure field, for the zero side-slip condition, both with and without the LEX fence. The LEX fence significantly reduces the magnitude of the rms pressures and bending moments. Scaling issues are addressed by comparing full-scale results for pressures at the 60%-span and 45%-chord location with small-scale, F/A-18 tail-buffet data. The comparison shows that the tail buffet frequency scales very well with length and velocity. Root-mean-square pressures and power spectra do not scale as well. The LEX fence is shown to reduce tail buffet loads at all model scales.

Nomenclature

C_p' = rms pressure coefficient, $p'/\frac{1}{2}\rho V^2$
C_p'' = pressure power coefficient, $4p''/lp^2V^3$
F = reduced frequency, lf/V
f = frequency, Hz
l = characteristic length scale, ft
p' = rms pressure, psi
p'' = pressure power, psi^2/Hz
V = velocity, ft/s
α = angle of attack, deg
ρ = density, slugs/ft^3

Introduction

TAIL buffet occurs when the vortex shed from a strake or a leading-edge extension (LEX) bursts immediately forward of the tail. Although tail buffet can be a problem for any aircraft, it is a special concern for twin-tailed fighter aircraft. The F/A-18, in particular, had serious fatigue problems because of tail buffeting until a vertical plate, referred to as the LEX fence, was developed and installed on the aircraft (Fig. 1). To show the effect of the LEX fence on tail buffeting, this article presents tail buffet data for the aircraft at zero sideslip, both with and without the LEX fence. Several studies of F-18 tail buffeting have also been carried out in small-scale tests[1–5] and in numerical simulations.[6,7] Tail buffet predictions based on small-scale test results have also been explored.[1,8,9]

The first full-scale F/A-18 wind-tunnel test (Fig. 2) was conducted as part of NASA's High Alpha Technology Program (HATP). The objective of the HATP program is to provide new technology and to validate design methods for the next generation of highly maneuverable aircraft. The HATP program encompasses several research efforts within NASA that include small-scale wind-tunnel and water-tunnel tests, flight tests with the High Angle-of-Attack Research Vehicle (HARV), computational fluid dynamic (CFD) computations, and the full-scale wind-tunnel tests conducted in the 80 by 120 ft Wind Tunnel. In addition to the tail buffet studies, the full-scale F/A-18 wind-tunnel tests include studies of forebody vortex control devices, CFD validation studies, and the compilation of surface pressure and force data to compare to small-scale tests and to flight. These studies will continue in future tests of the F/A-18 in the 80 by 120 ft Wind Tunnel. A survey of the results obtained in the first full-scale F/A-18 wind-tunnel test is given in Ref. 10.

The three principle objectives of the full-scale tail buffet tests are as follows:

1) Study the flowfield characteristics of tail buffet over a wide range of angle of attack and sideslip.

2) Quantify the effects of the LEX fence in reducing tail buffet loads.

3) Provide full-scale data to compare with data obtained in small-scale wind tunnels.

The goal of the first objective is to understand how angle of attack and sideslip affect tail buffet loads on twin-tailed aircraft. The data obtained will also be used to determine tail loading conditions for full-scale structural fatigue tests of the F/A-18 (Ref. 2). The goal of the second objective is to understand why the LEX fence reduces tail buffet loads. This information could lead to the development of alternative methods to reduce tail buffet loads. Finally, the goal of the last objective is to aid in the development of guidelines to quan-

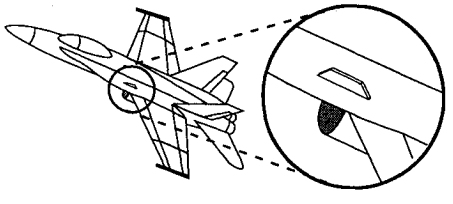

Fig. 1 F/A-18 LEX fence.

Presented as Paper 93-3519 at the AIAA 11th Applied Aerodynamics Conference, Monterey, CA, Aug. 9–11, 1993; received May 10, 1994; revision received Nov. 16, 1995; accepted for publication Nov. 20, 1995.

*Aerospace Engineer, Low Speed Aerodynamics Branch. Member AIAA.

†Aerospace Engineer, Scientific Systems Division. Member AIAA.

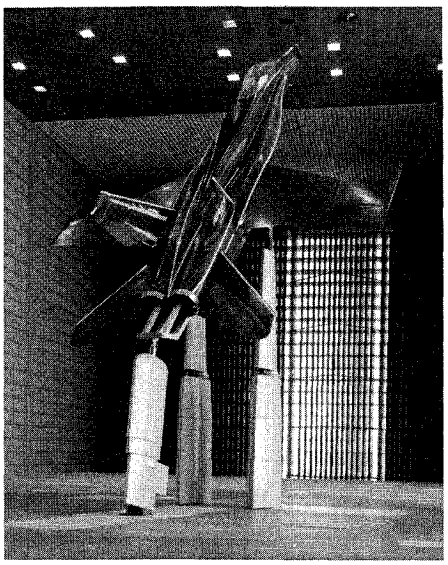

Fig. 2 F/A-18 in the 80 by 120 ft Wind Tunnel.

titatively predict tail buffet loads in flight from small-scale wind-tunnel data. To address this objective, pressure transducers were located on the full-scale aircraft in many of the same locations used in small-scale tests, allowing direct comparisons of full-scale data with data obtained at small scale. Several comparisons of full-scale data with published small-scale data are presented in this article.

Experimental Setup

Wind Tunnel

The 80 by 120 ft Wind Tunnel is part of the National Full-Scale Aerodynamic Complex (NFAC) located at NASA Ames Research Center.[11] The NFAC can be configured as either a closed-circuit wind tunnel with a 40 by 80 ft test section or an open-circuit wind tunnel with an 80 by 120 ft test section. A schematic of the facility is shown in Fig. 3. The maximum dynamic pressure attainable in the 80 by 120 ft Wind Tunnel is 33 psf, providing a maximum velocity of approximately 100 kn. The wind tunnel is driven by six 40-ft-diam, variable-speed, variable-pitch fans. Each fan is powered by a 22,500-hp electric motor and at full speed the wind tunnel draws 106 MW of power.

The aircraft was supported in the wind-tunnel test section by the three struts shown in Figs. 2 and 4. The two, fixed height, main struts were connected by a horizontal cross-bar. The aircraft was attached to the cross-bar with two blade and clevis assemblies that replaced the main landing gear trunnions. The tail strut is a large linear actuator that pitches the aircraft about main strut attachment pivots. To maintain a positive mechanical advantage at higher angles of attack, it was necessary to attach the tail strut to a point aft of the aircraft. This was achieved with a cantilevered structure connected to the F/A-18 engine mounts and to the arresting hook pivot (Figs. 2 and 4).

The three struts are mounted on a rotatable turntable that is supported by a six-component scale system. Each strut has a nonmetric aerodynamic fairing mounted on a nonmetric turntable that tracks the balance turntable. The fairings rotate to stay aligned with the wind-tunnel axis when the turntable rotates to yaw the aircraft. The fairing for the tail strut changes length and tilt angle to follow the tail strut when the aircraft is pitched.

Test Article

The aircraft, supplied by the U.S. Navy, is from the first F/A-18 model A production block. The aircraft engines and

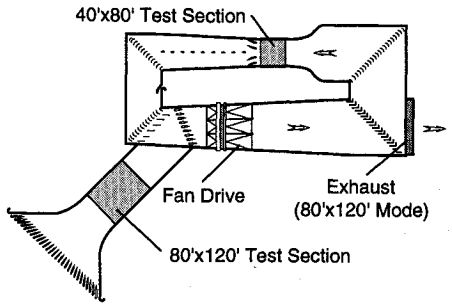

Fig. 3 Schematic of the National Full-Scale Aerodynamic Complex.

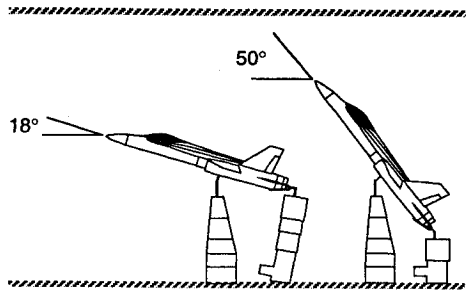

Fig. 4 Aircraft on struts for minimum and maximum angle of attack.

avionics were removed prior to shipment to Ames Research Center. The aircraft is 56.0 ft long, has a wingspan of 37.42 ft, the reference wing area is 400 ft^2, and the mean aerodynamic chord is 11.52 ft. Figure 4 is a schematic showing the aircraft in the 80-ft-high test section at the minimum and maximum angles of attack for this test. The aircraft was mounted slightly below the centerline of the test section to reduce the effect of ceiling proximity on the forebody at high angles of attack. Wind-tunnel blockage at 20-deg angle of attack is slightly less than 4.9% and climbs to less than 7.5% for an angle of attack of 50 deg.

The aircraft was configured with flow-through inlets. The aircraft missile rails were left in place, however, no missiles were attached. The aircraft had removable LEX fences (Fig. 1), which are installed on all U.S. Navy F/A-18 aircraft to reduce tail buffet loads. The LEXs used in this test were the pressure-instrumented pair normally flown on the HARV. The LEX fences are trapezoidal in shape, 8.375 in. high, 36.6 in. long at the base, and 27.9 in. long at the top.

The leading-edge flaps were fixed at a 33-deg deflection angle and trailing-edge flaps were fixed in their undeflected position. These flap deflections match the standard control-law schedule for angles of attack greater than 26 deg. The rudders were fixed in their undeflected position. The horizontal stabilators were actuated and their position was varied with angle of attack to match the trimmed stabilator positions of the HARV in steady, 1-g flight conditions.

Instrumentation

The tail-buffet instrumentation consisted of 32 15-psia pressure transducers, eight accelerometers, six strain gauges, and a surface temperature sensor. The pressure transducers were mounted on the surface of the left vertical tail in a 4 by 4 matrix on both the inboard and outboard surfaces (Fig. 5). Each vertical tail and each horizontal stabilator had two accelerometers mounted at their tips near the leading and trailing edges. The strain gauges were attached to the attachment stubs of the two vertical fins and the temperature sensor attached to the surface of the left vertical fin. Data were sampled at a rate of 512 Hz per channel for a period of 32 s. To eliminate concerns for frequency damping because of pressure lines, and to ease transducer installation, absolute pressure transducers that

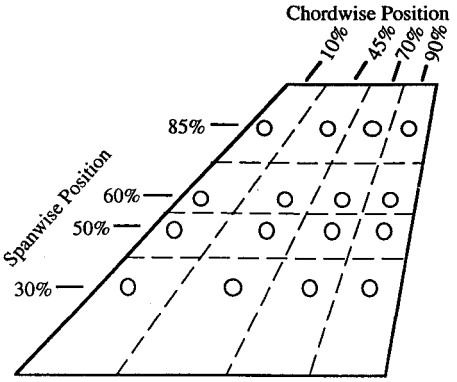

Fig. 5 Pressure transducer locations, left vertical fin.

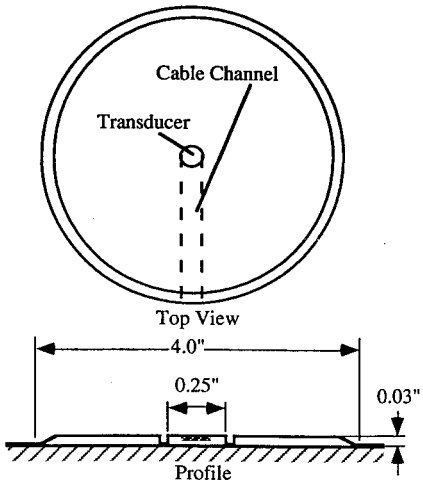

Fig. 6 Pressure transducer fairing.

did not have reference pressure lines were installed on the tail surface. Fairings, depicted in Fig. 6, were mounted around each pressure transducer to eliminate pressure disturbances because of the transducers obstructing the flow. The signals from the pressure transducers were ac coupled to eliminate the large dc offset caused by atmospheric pressure, and thereby allowing greater signal gain for increased resolution of the unsteady pressures measured. Smoke flow visualization and laser light sheets were used to determine the location of the LEX vortex and its burst position.

Test Conditions

Most of the test was conducted at a freestream velocity of 168 ft/s. This corresponds to a dynamic pressure of 33 psf, a Mach number of 0.15, and a Reynolds number of 12.3×10^6 based on mean aerodynamic chord. The lowest velocity tested was 65 ft/s, which corresponds to a dynamic pressure of 5 psf. The angle of attack ranged from 18 to 50 deg and the angle of sideslip ranged from -15 to 15 deg. Only data from the zero sideslip condition are presented in this article. The dynamic pressure was about an order of magnitude less than at the flight conditions where tail buffeting results in significant motion of the tail. Accelerometers confirmed that tail motion in this test was negligible, and therefore, the results presented should be considered rigid tail results. The burst position of the LEX vortex vs angle of attack was consistent with small-scale wind-tunnel test results and with flight-test results.[12]

Analysis Methods

Data Reduction

The method chosen to estimate the power spectral distribution (PSD) was a single-sided periodogram utilizing a fast Fourier transform (FFT) algorithm. This is a classical method of PSD estimation, and it has the advantage that the integral of the estimated PSD with respect to frequency is equal to the variance [or the rms (Ref. 2)] of the signal. To determine a time-averaged PSD, the 32-s time record, which contained 16,384 samples, was subdivided into 127 half-second time records that overlapped by 50%. A Hann window was applied to each record, which contained 256 samples, and then, to regain some frequency resolution, each record was padded with zeros to increase the record length to 4096. PSDs were calculated for each record and averaged to yield a time-averaged PSD.

Differential pressures were calculated by subtracting the inboard pressure value from the corresponding outboard pressure for each time step. To calculate bending moments caused from buffet pressure, the surface area of the vertical fin was divided as shown in Fig. 5. The differential pressures measured at the transducer locations shown were multiplied by the area of the enclosing subsection and by the distance of the subsection centroid from the fin root. These values for all 16 subsections were then summed for each time step to obtain a time history for the bending moment imposed by the pressure field on the fin. The array of pressure transducers was too sparse to obtain the correct bending moment magnitude by this method.[13,14] However, the differences in the relative magnitude of these bending moments are valid and show important trends. For these reasons, the bending moment results are presented in this article with the scaling information removed.

Nondimensional Parameters

The derivations of the nondimensional parameters for frequency, rms pressure, and buffet pressure PSDs are given in Ref. 1. The definitions for F, C_p', and C_p'' are given in the Nomenclature. For this article the mean aerodynamic chord (11.52 ft) was chosen as the l, and the free stream velocity was chosen as V.

Measurement Uncertainty

Based on a 95% confidence level, the uncertainty in the dimensional and nondimensional pressure measurements was estimated to be $\pm 6\%$. The uncertainty in estimated PSD values was estimated to be $\pm 19\%$, which was primarily because of the short time records used. An estimate for uncertainty in the values for peak frequency was not attempted because of the difficulty of the task. However, it should be noted that uncertainty in the peak frequency is a function of the peak power level and the uncertainty tends to increase as the peak power level decreases. These uncertainties are presented as error bars on all of the data figures except for those displaying peak frequency.

Experimental Results

LEX Fence Effect

Figure 7 shows bending moment power spectra for the port-side vertical tail for angles of attack from 20 to 40 deg. The data repeatability is demonstrated in Figs. 7a, 7c, and 7f. As shown, the LEX fence is an effective means of reducing the bending moment power up to an angle of attack of 32 deg. Flow visualizations that were conducted during the test indicated that the LEX vortex bursts well ahead of the LEX fence position for angles of attack greater than 35 deg. For these angles of attack, the buffeting that occurs may also be partly because of the wake of the wing and fuselage. The LEX fence retains some effectiveness at 35 deg (Fig. 7e); however, there is no evident LEX fence effect at 40 deg (Fig. 7f). Although the data are not presented here, there is no evident LEX fence effect at 45- and 50-deg angle of attack.

Figure 8 shows the variation in rms bending moment with angle of attack. The LEX fence reduces the variation in the peak power with angle of attack for the time-averaged bending moment power spectra. The LEX fence reduces peak power

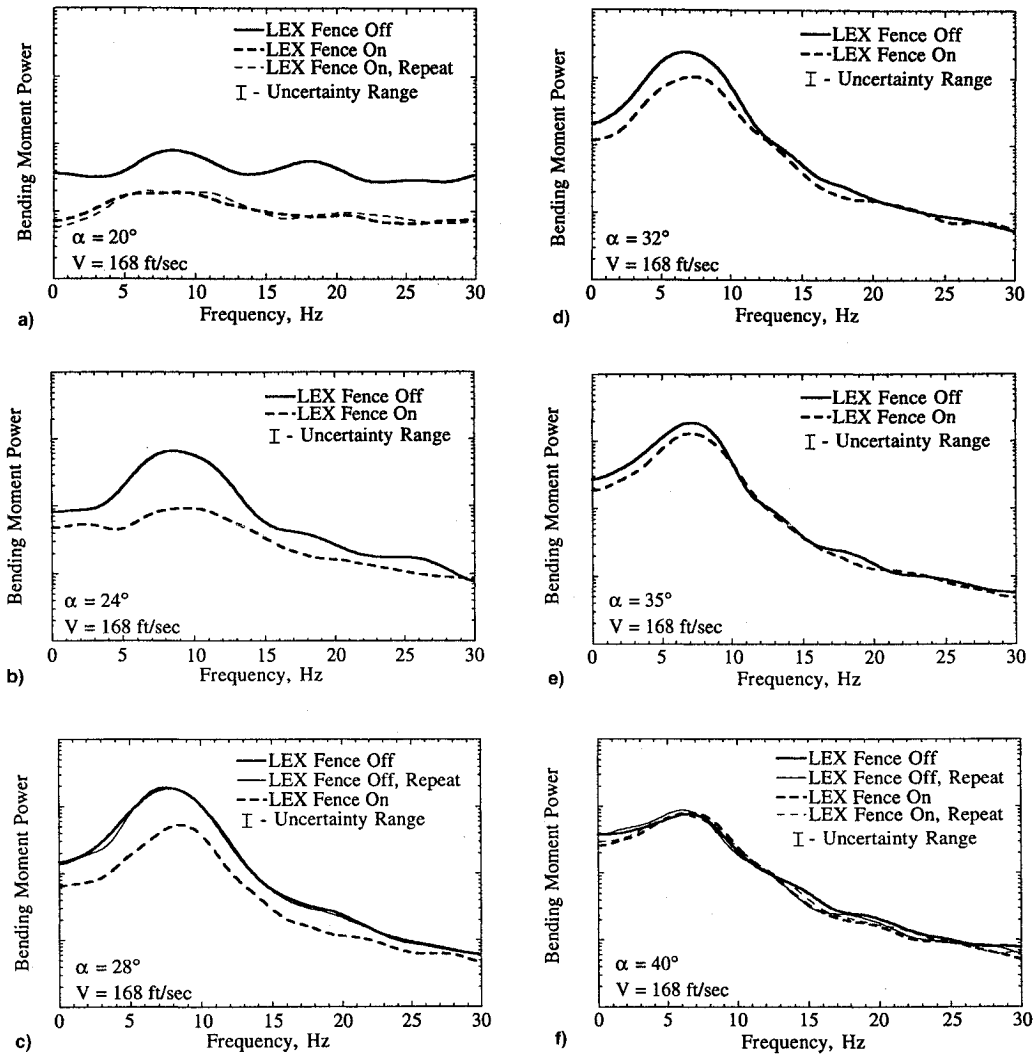

Fig. 7 Bending moment power spectra for α = 20–40 deg; both with and without the LEX fence.

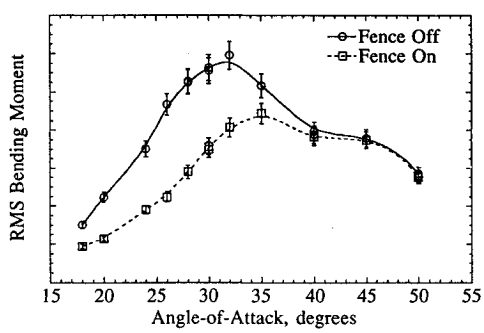

Fig. 8 Variation of rms bending moment with angle of attack.

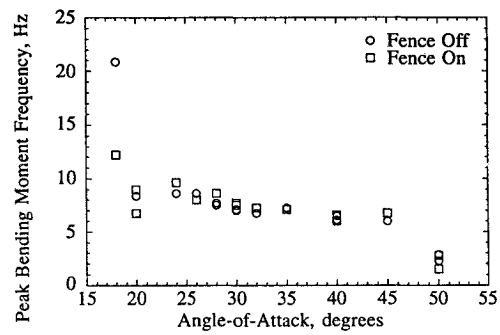

Fig. 9 Variation of peak bending moment frequency with angle of attack.

for angles of attack less than 40 deg and the magnitude of the maximum peak power attained is reduced by nearly 50%. The frequency of the peak power, shown in Fig. 9, is not significantly affected by the LEX fence. Frequency data for angles of attack less than 24 deg are scattered because the power spectra did not contain clearly defined and repeatable peaks.

Scale Effects

Small-scale tests have shown that tail buffet power spectra scale very well with velocity.[1] This is also true for the full-scale test. Figure 10 presents the nondimensional PSDs for the pressure transducer at the 60% span, 45% chord, inboard location for velocities of 168 and 130 ft/s. The excellent agreement exhibited over the entire frequency range indicates that velocity scaling is valid at full-scale test conditions.

The comparisons of full- with small-scale data presented in this article are for the 60% span and 45% chord location. First, comparisons between full-, and 12%-scale[1] differential pressure data are presented. Then, comparisons between full-, 16%- (Ref. 3), and 6%-scale[5] inboard and outboard pressure data are presented. Data for both the LEX fence off and on are presented where available.

Figure 11 shows comparisons of nondimensional power spectra from the full- and 12%-scale tests for angles of attack from 24 to 36 deg. Full-scale data were not available for 36

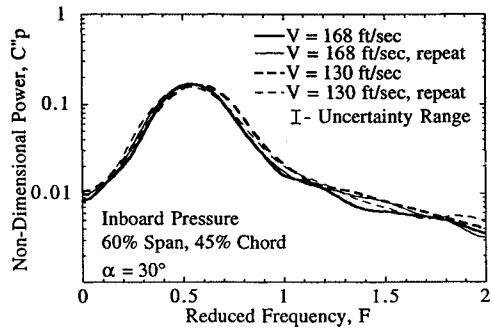

Fig. 10 Nondimensional power spectra for two velocities.

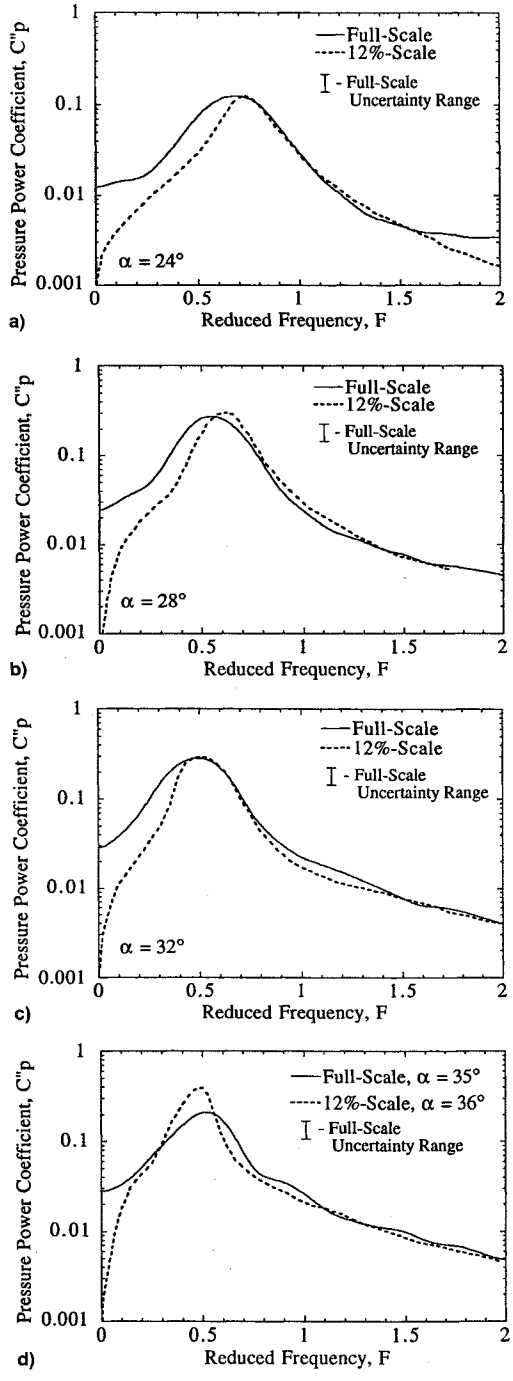

Fig. 11 Differential pressure power at 60% span and 45% chord on the vertical tail of the full-scale and 12%-scale models. α = a) 24-deg, b) 28-deg, c) 32-deg, and d) 35-deg full-scale/α = 36-deg 12% scale.

deg, and so data for 35 deg are shown. The power spectra for 24, 28, and 32 deg (Figs. 11a–11c) show good agreement for frequencies at and above the peak in the PSD, but the full-scale power spectra have more power in the lower frequencies. The comparison between the power spectra for 35 and 36 deg (Fig. 11d) shows that the peak power for the 12% scale is significantly greater than that for the full scale. This peak seems somewhat anomalous, and it may indicate that something unusual may have occurred at 36-deg angle of attack on the small-scale model that did not occur for the full-scale test. The differences in power levels at the low frequencies may be because of low-frequency noise sources in the full-scale facility and/or mounting hardware, or it is very possible that it is because of differences in data reduction.

Figure 12 shows the reduced frequency of the peaks in the differential pressure power spectra, for the full scale and 12% scale. The full-scale frequency is in good agreement with the 12%-scale frequency up to 45-deg angle of attack. At 50 deg, the full-scale frequency drops below the frequencies shown for the 12%-scale model at 48- and 52-deg angle of attack. The LEX fence, at full scale, is shown to have negligable effect on reduced frequency.

Figure 13 shows that the full-scale rms pressure coefficients are noticeably higher than those of the 12% scale at angles of attack less than 35 deg. At 35-deg angle of attack and greater, the full-scale and 12%-scale rms pressure coefficients are in very good agreement. The LEX fence, at full scale, is shown to reduce the differential rms pressure at 35-deg angle of attack and lower.

The peak differential PSD pressure coefficient is shown in Fig. 14 as a function of angle of attack. The coefficients agree remarkably well for full scale and 12% scale, except for the 12%-scale points at 36- and 44-deg angle of attack. The full-scale data show a relatively smooth variation in peak power with angle of attack and the peak power decreases for angles of attack greater than 32 deg. The 12%-scale data show the peak power leveling off around 28- and 32-deg angle of attack and then jumping abruptly for 36 deg. This indicates that something unusual is happening around 36-deg angle of attack

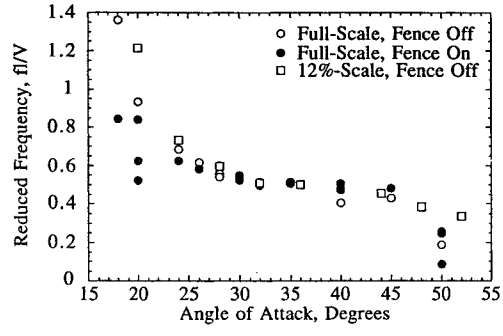

Fig. 12 Nondimensional peak power frequency for differential pressure at 60% span and 45% chord on the vertical tail.

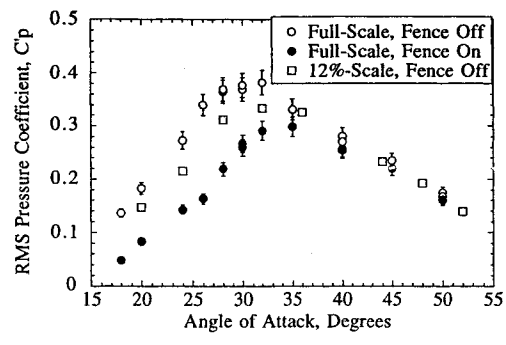

Fig. 13 Root-mean-square pressure coefficient for differential pressure at 60% span and 45% chord on the vertical tail.

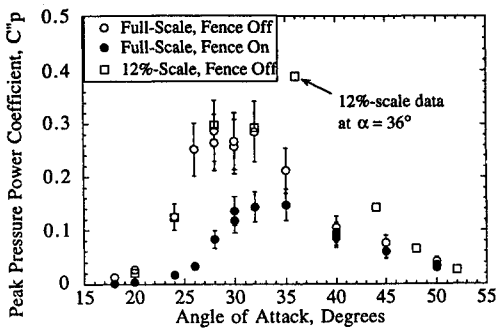

Fig. 14 Peak pressure power coefficient for differential pressure at 60% span and 45% chord on the vertical tail.

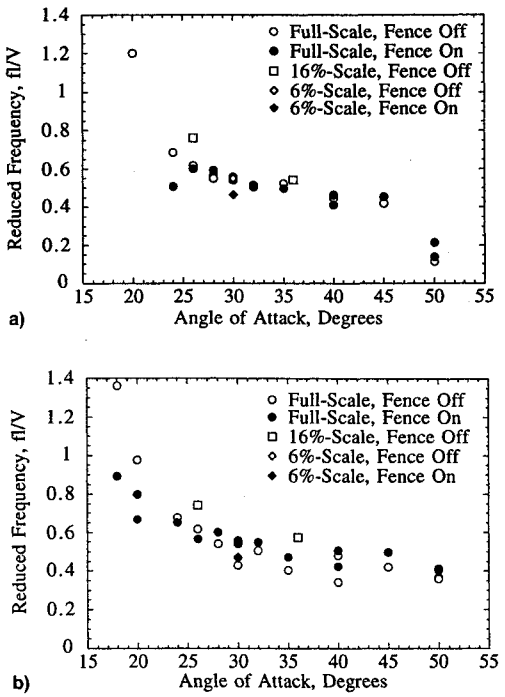

Fig. 15 Nondimensional peak power frequency for a) inboard and b) outboard pressures at 60% span and 45% chord on the vertical tail.

for the 12% scale, that does not occur at full scale. The LEX fence, at full-scale, is shown to significantly reduce the peak differential PSD pressure at 35-deg angle of attack and lower. The overall maximum differential PSD pressure is reduced by 50% with the LEX fence on.

Comparisons of full-scale inboard and outboard pressure data with 16- and 6%-scale data are shown in Figs. 15 and 16. Figure 15a shows the reduced frequency of the peaks in the inboard pressure power spectra, and Fig. 15b shows the reduced frequency for the outboard pressure. The full-scale data in both figures exhibit more scatter than was shown for the frequencies found for differential pressure (Fig. 12). The large amount of scatter makes it difficult to draw any clear conclusions from the data presented in Fig. 15. However, the 16%-scale frequencies are consistently higher than the full- and 6%-scale frequencies in both Figs. 15a and 15b.

Figure 16a shows the rms pressure coefficient for inboard pressure data. The full-scale rms pressure coefficient is consistently greater than small scale for angles of attack less than 36 deg. At 36 deg, the 16% scale has a slightly higher rms pressure coefficient. The effect of the LEX fence at all three scales is to reduce the rms pressure for angles of attack of 36 deg and less. The outboard rms pressure coefficients (Fig. 16b) are lower than the inboard rms pressures in the angle-of-attack range from 24 to 45 deg. The scatter in the data shown in Fig.

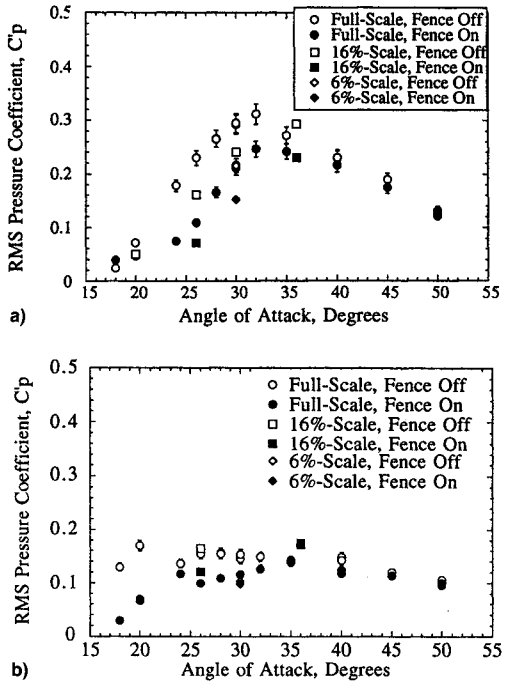

Fig. 16 Root-mean-square pressure coefficient for a) inboard and b) outboard pressures at 60% span and 45% chord on the vertical tail.

16b makes it difficult to draw any clear conclusions about the differences between model scales or about the effect of the LEX fence. Overall, the inboard pressure would seem to contribute more to tail buffet loads than does the outboard pressure.

Note that the model support struts used in this test may have influenced the results in some unknown manner. It would be expected that the support strut interference would be the worst for high angles of attack where the tails are closer to the wakes of the support struts; however, the agreement with small-scale test seems to be the best at these angles of attack.

Concluding Remarks

The LEX fence significantly reduces rms bending moment and peak PSD bending moment. It also significantly reduces rms pressure and peak PSD pressure at all model scales. The LEX fence did not significantly affect the peak power frequency.

Nondimensional peak power frequencies measured in small-scale tests agree well with the full-scale frequencies. However, nondimensional rms pressures measured on the full-scale aircraft were greater than those measured in small-scale tests for angles of attack less than 40 deg. Comparisons of the nondimensional power spectra for the full-scale aircraft and the 12%-scale model show that the full-scale power spectra have more power in the frequencies below the peak power frequency. Above this frequency, the nondimensional power spectra for both model scales are in good agreement.

References

[1]Zimmerman, N. H., and Ferman, M. A., "Prediction of Tail Buffet Loads for Design Application," Naval Air Development Center 88043-60, July 1987.

[2]Martin, C. A., Glaister, M. K., MacLaren, L. D., Meyn, L. A., and Ross, J., "F/A-18 1/9th Scale Model Tail Buffet Measurements," Aeronautical Research Lab., Flight Mechanics Rept. 188, Melbourne, Australia, June 1991.

[3]Shah, G. H., "Wind-Tunnel Investigation of Aerodynamic and Tail Buffet Characteristics of Leading-Edge Extension Modifications to the F/A-18," AIAA Paper 91-2889, Aug. 1991.

[4]Shah, G. H., Grafton, S. B., Guynn, M. D., Brandon, J. M., Dans-

berry, B. E., and Patel, S. R., "Effect of Vortex Flow Characteristics on Tail Buffet and High-Angle-of-Attack Aerodynamics of a Twin-Tail Fighter Configuration," High-Angle-of-Attack Technology Conf., Oct. 1990.

[5]Lee, B. H. K., and Brown, D., "Wind-Tunnel Studies of F/A-18 Tail Buffet," *Journal of Aircraft*, Vol. 29, No. 1, 1992, pp. 146–152.

[6]Rizk, Y. M., and Gee, K., "Numerical Prediction of the Unsteady Flowfield Around the F-18 Aircraft at Large Incidence," AIAA Paper 91-0020, Jan. 1991.

[7]Rizk, Y. M., Guruswamy, G. P., and Gee, K., "Computational Study of F-18 Vortex Induced Tail Buffet," AIAA Paper 92-4699, Sept. 1992.

[8]Washburn, A. E., Jenkins, L. N., and Ferman, M. A., "Experimental Investigation of Vortex-Fin Interaction," AIAA Paper 93-0050, Jan. 1993.

[9]Jacobs, J. H., Hedgecock, C. E., Lichtenwalner, P. F., Pado, L. E., and Washburn, A. E., "The Use of Artificial Intelligence for Buffet Environments," *AIAA 34th Structures, Structural Dynamics, and Materials Conference*, AIAA, Washington, DC, 1993, pp. 1592–1960.

[10]Meyn, L. A., Lanser, W. R., and James, K. D., "Full-Scale High Angle-of-Attack Tests of an F/A-18," AIAA Paper 92-2676, June 1992.

[11]Corsiglia, V. R., Olson, L. E., and Falarski, M. D., "Aerodynamic characteristics of the 40- by 80/80- by 120-Foot Wind Tunnel at NASA Ames Research Center," NASA TM 85946, April 1984.

[12]Meyn, L. A., and Bennett, M. S., "Application of a Two Camera Video Imaging System to Three-Dimensional Vortex Tracking in the 80- by 120-Foot Wind Tunnel," AIAA Paper 93-3439, Aug. 1993.

[13]James, K. D., and Meyn, L. A., "Dependence of Integrated Vertical-Tail Buffet Loads for F/A-18 on Sensor Density," ISAE Aerospace Atlantic Conf., Society of Automotive Engineers Paper 941140, April 1994.

[14]Meyn, L. A., and James, K. D., "Integrated Tail Buffet Loads on the F/A-18," AIAA Paper 94-3439, June 1994.